Gene discovery by chemical mutagenesis and whole-genome sequencing in *Dictyostelium*

Cheng-Lin Frank Li,[1] Balaji Santhanam,[2] Amanda Nicole Webb,[1] Blaž Zupan,[1,3] and Gad Shaulsky[1]

[1]*Department of Molecular and Human Genetics, Baylor College of Medicine, Houston, Texas 77030, USA;* [2]*Graduate Program in Structural Computational Biology and Molecular Biophysics, Baylor College of Medicine, Houston, Texas 77030, USA;* [3]*Faculty of Computer and Information Science, University of Ljubljana, SI-1000 Ljubljana, Slovenia*

Whole-genome sequencing is a useful approach for identification of chemical-induced lesions, but previous applications involved tedious genetic mapping to pinpoint the causative mutations. We propose that saturation mutagenesis under low mutagenic loads, followed by whole-genome sequencing, should allow direct implication of genes by identifying multiple independent alleles of each relevant gene. We tested the hypothesis by performing three genetic screens with chemical mutagenesis in the social soil amoeba *Dictyostelium discoideum*. Through genome sequencing, we successfully identified mutant genes with multiple alleles in near-saturation screens, including resistance to intense illumination and strong suppressors of defects in an allorecognition pathway. We tested the causality of the mutations by comparison to published data and by direct complementation tests, finding both dominant and recessive causative mutations. Therefore, our strategy provides a cost- and time-efficient approach to gene discovery by integrating chemical mutagenesis and whole-genome sequencing. The method should be applicable to many microbial systems, and it is expected to revolutionize the field of functional genomics in *Dictyostelium* by greatly expanding the mutation spectrum relative to other common mutagenesis methods.

[Supplemental material is available for this article.]

The social amoeba, *Dictyostelium discoideum,* is a eukaryote that grows as a unicellular organism and develops as a multicellular organism. It is used in a wide array of biomedical and basic biology research (Annesley and Fisher 2009; Williams 2010). Early genetic studies in *Dictyostelium* utilized chemical mutagens or UV irradiation to generate mutants. Although it is possible to map causative mutations to linkage groups by parasexual genetics, most of the target genes have not been identified because recombination is very limited under these conditions (Loomis 1987). Restriction enzyme-mediated integration (REMI) mutagenesis, which allows researchers to tag and clone the target genes in forward genetic screens, replaced chemical mutagenesis in the 1990s (Kuspa and Loomis 1992). Since then, REMI has been the workhorse of gene discovery in *Dictyostelium*. Other techniques, including gene silencing by antisense RNA (Spann et al. 1996) and by RNA interference (RNAi) (Kuhlmann et al. 2006), have been developed, too, but they are not commonly used in *Dictyostelium* research.

We wanted to resurrect the use of chemical mutagenesis and integrate it with whole-genome sequencing in forward genetic screens for three major reasons. First, chemical mutagenesis generates a broad spectrum of mutant alleles. The mutations can generate gain-of-function, temperature sensitive, and null alleles. They can also generate subtle variations that would facilitate the study of protein structure and function (Loomis 1987). Secondly, *Dictyostelium* has a very gene-rich, haploid genome of 34 Mb (Eichinger et al. 2005), which is readily amenable to high-throughput sequencing technologies, especially with the low cost afforded by sample multiplexing. Lastly, we found that REMI suppressors are rare and weak in previous screens for suppressors of the *tgrC1*-defective phenotypes (Li et al. 2015; Wang and Shaulsky 2015), and we wanted a method that would generate a variety of stronger suppressor mutations.

The major challenge in chemical mutagenesis stems from the large number of mutations induced per genome, which requires implementation of tedious genetic mapping techniques to locate the causative mutation to a defined genomic region (Sarin et al. 2008; Haelterman et al. 2014). Here, we report on a method for identification of chemical-induced mutations in *Dictyostelium*. First, we limited the number of mutations per genome by titrating the dose of the chemical mutagen. Next, we identified multiple mutant strains with common phenotypes. We then utilized sample multiplexing to reduce the whole-genome sequencing costs and developed a data analysis pipeline to identify, filter, and annotate mutations at a genomic scale. We implicated the target genes by recovering multiple mutant alleles and successfully identified and validated the causative mutations, thereby bypassing the need for genetic mapping. This chemical mutagenesis-based gene discovery pipeline is a significant addition to *Dictyostelium* genetics and is additionally applicable to other organisms.

Results

Genetic screens with chemical mutagenesis span a wide range of relevant target sizes

We performed genetic screens to test the limits of the system, one in which the number of possible genes (relevant target size) was

Corresponding author: gadi@bcm.edu
Article published online before print. Article, supplemental material, and publication date are at http://www.genome.org/cgi/doi/10.1101/gr.205682.116.

26:1268–1276 Published by Cold Spring Harbor Laboratory Press; ISSN 1088-9051/16; www.genome.org

small and one in which it was large. We induced mutations by exposing *Dictyostelium* cells to *N*-methyl-*N*′-nitro-*N*-nitrosoguanidine (NTG). In the first screen, we selected for resistance to light-induced cell death. The predicted targets were genes that encode biosynthetic components of light-sensitive chromophores (e.g., flavins and porphyrins) (Godley et al. 2005), so we presumed a small target size even though this phenotype has not been investigated in *Dictyostelium* before. Figure 1A shows that wild-type cells grow well on bacteria in the dark but fail to grow under intense illumination. We isolated six mutants (four shown, Fig. 1A) that grow both in the dark and under intense light. The mutants grow slightly better in the dark, suggesting that the mutations do not completely protect them from the lethal effects of intense light.

In the second set of experiments, we performed a screen for an aggregation-less phenotype. *Dictyostelium* aggregation has been studied extensively, and the networks that regulate it contain 100–150 genes (Swaney et al. 2010), a rather large relevant target size. When amoebae grow on bacteria, they consume the bacteria and grow outwardly, forming an expanding circular plaque in the bacterial lawns around them. Cells in the center of the plaque starve as the bacteria are consumed, while cells at the edge of the plaque continue to grow. Starving wild-type cells then aggregate and develop into fruiting bodies (Fig. 1B). We isolated 14 mutants (five shown, Fig. 1B) that grew and cleared the bacterial lawns but remained flat even upon prolonged starvation, indicating failure to aggregate.

In the third set of experiments, we sought genes in a novel pathway, combining a selection with a visual screen for suppression of the *tgrB1-C1* mismatch phenotypes. TgrB1 and TgrC1 are cell-surface adhesion proteins that form heterophilic interactions *in trans* (Chen et al. 2013). Cells carrying a mismatched allelic pair of the *tgrB1* and *tgrC1* genes exhibit impaired cell-cell recognition and are unable to complete development (Benabentos et al. 2009; Hirose et al. 2011, 2015). The $tgrB1^{AX4}tgrC1^{QS38}$ cells carry a mismatched pair of alleles, so their development is arrested at the loose mound stage and they do not form spores (Fig. 1C; Hirose et al. 2011). Previous REMI mutagenesis screens yielded small numbers of weak suppressors (Li et al. 2015; Wang and Shaulsky 2015), so we did not know if it was even possible to generate strong suppressors, let alone the relevant target size. We mutated these cells, allowed the population to develop, and selected for spores by detergent treatment. We plated the survivors at low density on nutrient agar in association with bacteria and screened for mutants that formed fruiting bodies. We recovered 63 mutants that fulfilled these criteria (five shown, Fig. 1C), indicating that it is possible to obtain a large number of strong suppressors of the *tgrB1-C1* mismatch phenotype.

The three genetic screens verify previous reports that chemical mutagenesis can be used for identification of aggregation-less mutants (Williams and Newell 1976) and show that new phenotypes can be detected as well.

Low levels of chemical mutagenesis produce enough mutants for screening

We wanted to find conditions that would produce enough mutant strains for screening and selection while keeping a low number of mutations in each genome. Previous studies used conditions that resulted in low survival rates (Loomis 1987). It is hard to evaluate the number of mutations in each genome in those studies, but it was estimated at several hundred to several thousand. To evaluate the relationship between the number of mutations per genome and the number of mutants in the population, we measured the relationship between the duration of NTG treatment and the survival rate, as well as the relationship between survival rate and frequency of mutants with defined phenotypes. We found that survival was inversely correlated with the duration of NTG treatment (Fig. 1D) and that the frequency of mutants was inversely correlated with survival (Fig. 1E). We also found that it is possible to generate enough mutants for selections and screens even with high survival rates, suggesting that it would be possible to identify the causative mutations by whole-genome sequencing.

Whole-genome sequencing reveals a small number of variants per genome

We used high-throughput sequencing to analyze the genomes of the two parental strains (AX4 and $tgrB1^{AX4}tgrC1^{QS38}$) and the 83 mutants found in the three screens. We multiplexed the samples for cost effectiveness such that 16–24 strains were grouped in each sequencing lane. We obtained 15.8 ± 3.6 (mean ± standard deviation [SD]) million reads per genome and were able to map 99% of the reads to the reference genome with a mean fold-coverage of 19.4 ± 5.2 (mean ± SD) over the entire genome. The coverage of individual chromosomes is shown in Supplemental Figure S1A. To identify mutations, we performed multisample variant calling on single nucleotide variants (SNVs) and indels (McKenna et al. 2010). To remove false positive variants, we imposed three filters: read depth, allele frequency, and pre-existing variations in the parental strain. These filters removed 99% of the raw SNVs and indels (Table 1), leaving 16.3–29.7 SNVs and 0.1–1.0 indels per genome. The number of variants per genome was negatively correlated with survival (Fig. 2A). More specifically, survival rates of 30%, 10%, and 0.1% corresponded to an average of 13, 21, and 34 variants per genome, respectively. Since ~30% of the entire genome and ~10% of the coding exons did not pass the read depth filter and were therefore excluded from SNP calling (Supplemental Fig. S1B), we probably underestimated the number of NTG-induced mutations per genome. Nevertheless, this relatively small number of mutations per genome suggested that it would be possible to identify causative mutations by comparing the genome sequences of strains with similar phenotypes. Figure 2A also shows a diminishing returns relationship between survival and the number of variants per genome, suggesting that reducing the survival rate to 0.1% or below does not contribute significantly to mutant discovery.

Most SNVs cause missense mutations

Most of the NTG-induced SNVs we found are G > A or T > C transitions (G > A:T > C ratio = 19:1), consistent with the mutagenic action of NTG (Fig. 2B; Lucchesi et al. 1986; Ohta 2000). We classified the SNVs into eight categories (Fig. 2C). The majority of SNVs occurred in coding exons, which is expected because coding exons contain 71.7% of the G-C base pairs in the *Dictyostelium* genome (Eichinger et al. 2005). Statistical testing indicates significant enrichment of exonic mutations in two experiments (exact binomial test: 77.4% of the 416 SNVs in the aggregation defects experiment, P value < 0.01; 86.5% of the 1253 SNVs in the suppression of *tgrC1-B1* mismatch experiment, P value < 0.001). Moreover, the *Dictyostelium* codon usage bias predicts that 76.6% of the exonic G > A transitions would result in missense mutations. Indeed, our results show that the predominant type of exonic

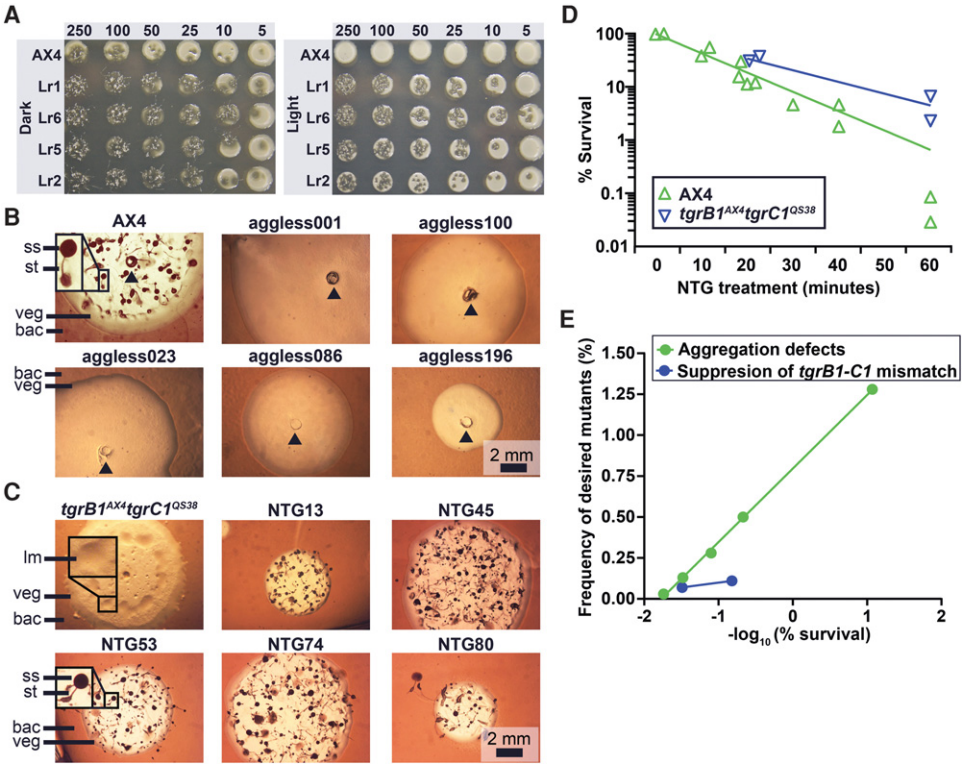

Figure 1. Genetic screens with chemical mutagenesis. (*A*) We compared the viability of the wild-type AX4 and the light-resistant (Lr#) mutants. We spotted 5 to 250 *Dictyostelium* cells on nutrient agar in association with bacteria. We incubated the plates in darkness (Dark) or under intense illumination (Light) for 4–5 d. Opaque circles are thick bacterial lawns (e.g., AX4, Light, 250) and dark plaques within the lawns are clearings that indicate amoebae growth. Whenever the amoebae cleared the bacterial lawns, starved and developed, a mass of fruiting bodies is evident as opaque spots and protrusions over the plaque background (e.g., Lr1, 250). (*B*,*C*) We inoculated the indicated *Dictyostelium* strains in association with bacteria (bac) on nutrient agar and incubated for 4–5 d. Cells (AX4 and NTG#) in the center of the plaque starved and developed into mature fruiting bodies with a sorus (ss) atop a stalk (st). Aggregation-less (aggless#) mutants did not form aggregates. *tgrB1*^{AX4}*tgrC1*^{QS38} cells arrested at the loose mound (lm) stage. Vegetative (veg) *Dictyostelium* cells resided in the translucent periphery of the plaque. *Insets* are magnified (3×) for visual clarity. The black arrowheads indicate inoculation spots. Scale bar = 2 mm. (*D*) We measured the survival rate (%, *y*-axis) over time (minutes, *x*-axis) during mutagenesis of two strains, AX4 ($n = 13$) and *tgrB1*^{AX4}*tgrC1*^{QS38} ($n = 4$). (*E*) We measured the frequency (%, *y*-axis) of mutants with the desired phenotypes and plotted against the negative logarithm of survival (%, *x*-axis) in the genetic screens for aggregation defects ($n = 5$) and for suppression of the *tgrB1-tgrC1* mismatch phenotype ($n = 2$).

mutations is missense, with significant enrichment in two experiments (exact binomial test: 82.0% of the 322 exonic mutations in the aggregation defects experiment, P value = 0.02; 82.0% of the 1084 exonic mutations in the suppression of *tgrC1-B1* mismatch experiment, P value < 0.001). Nonsense mutations occurred at 3.2%–7.1%, with a frequent occurrence in the glutamine codon (CAA > TAA, 60%). Figure 3 shows the locations of the mutations, suggesting that NTG-induced mutations are randomly distributed throughout the genome (Kolmogorov-Smirnov test for uniformity: light resistance, P value = 0.2314; aggregation defects, P value = 0.2545; suppression of *tgrC1-B1* mismatch, P value = 0.1757). We conclude that NTG-induced mutations are distributed nearly randomly throughout the genome and are most likely to modify protein-coding genes.

Multiple mutations in the ALA synthase gene, *hemA*, in light-resistant mutants

To identify phenotype-causing mutations, we looked for genes that were mutated independently in multiple strains with common phenotypes. We recovered six light-resistant strains (Table 1) and found that *hemA* was mutated independently in four of

Table 1. Filtering variants found in whole-genome sequencing

	Light resistance	Aggregation defects	Suppression of *tgrB1-tgrC1* mismatch
Parental strain	AX4	AX4	*tgrB1*^{AX4}*tgrC1*^{QS38}
Number of strains	6	14	63
Raw SNVs	27,187	33,378	78,269
Raw indels	3078	4510	8012
SNVs that passed filters	98	416	1253
Indels that passed filters	6	10	7
SNVs per genome (mean ± SD)	16.3 ± 8.4	29.7 ± 11.2	19.9 ± 11.7
Indels per genome (mean ± SD)	1.00 ± 1.26	0.71 ± 0.99	0.11 ± 0.44

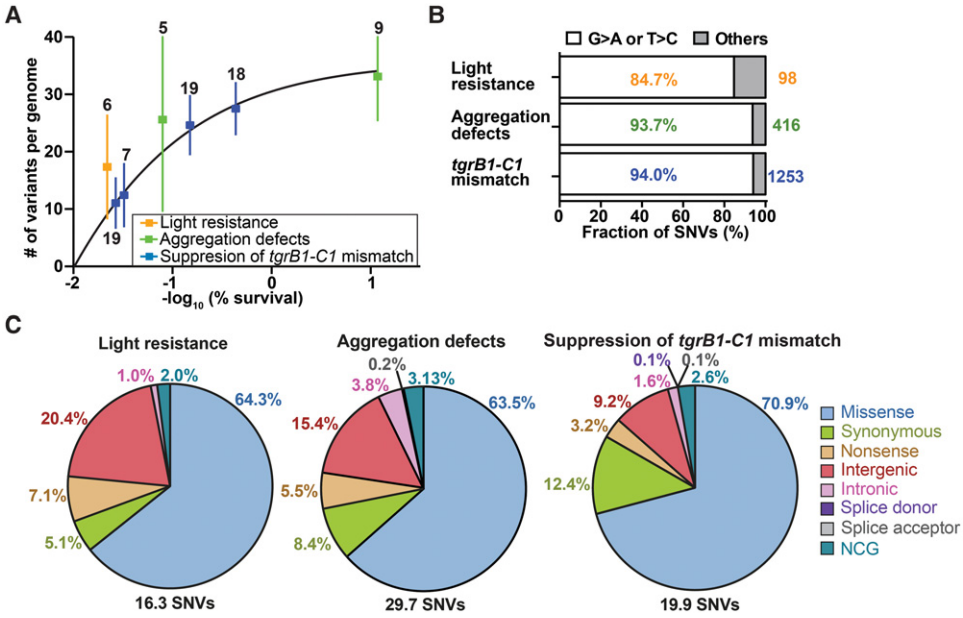

Figure 2. Properties of the chemically induced mutations. (*A*) We plotted the number of mutations (single nucleotide variants and indels) per genome (*y*-axis) against the negative logarithm of survival (%, *x*-axis). Dots represent means and whiskers represent 95% confidence intervals. Sample sizes are indicated next to each whisker, and the framed legend describes the experiments. (*B*) The bars show the proportion of filtered single nucleotide variants (SNVs) that are G > A or T > C transitions in individual experiments (white) and the other substitutions (gray). Percentages of G > A or T > C transitions are indicated *inside* the bars. The total numbers of filtered SNVs are indicated on the *right*. Sample size: light resistance ($n = 6$), aggregation defects ($n = 14$), and *tgrB1-C1* mismatch ($n = 63$). (C) SNVs were classified into eight groups based on the locations and types of substitution mutations (missense, synonymous, nonsense, intergenic, intronic [excluding splice sites], splice donor site, splice acceptor site, and NCG [noncoding gene], as indicated on the *right*). Titles *above* the pie charts describe the experiments. The average number of SNVs per genome is indicated on the *bottom*. The percentages of individual mutation types are indicated next to individual sectors.

them (Fig. 3; Supplemental Table S1). None of the other genes mutated in this screen was common to two or more strains.

hemA encodes the *D. discoideum* 5-aminolevulinate (ALA) synthase. ALA is a precursor in heme biosynthesis (Ajioka et al. 2006) and intense illumination damages cells by causing ALA-induced porphyrin accumulation and intra-cellular ROS production (Godley et al. 2005). ALA is photosensitive and its derivatives are used as photosensitizers in photodynamic therapy (Dolmans et al. 2003). Our finding of multiple mutations only in *hemA* and the known role of ALA in photosensitivity implicate the mutations in *hemA* as the cause of the light-resistance phenotype. The two strains that do not carry mutations in *hemA* suggest that other genes are also involved. Most importantly, these results demonstrate that we can reach near-saturation and identify recurrent mutations in a genetic screen over a small relevant target size.

Known aggregation genes found in a screen for aggregation defects

Dictyostelium aggregation involves more than 110 genes (Swaney et al. 2010), so we did not expect to reach saturation with only 14 mutants (Table 1). Nevertheless, we did expect to find mutations in some of the known genes among the aggregation-less mutants. Indeed, we identified one variant each in 13 aggregation-related genes (Supplemental Table S1). We also identified two or more variants each in five other genes (*tor*, *splA*, *DDB_G0275861*, *DDB_G0283339*, and *DDB_G0283893*) (Fig. 3; Supplemental Table S1). Only one of them, *tor,* has been previously implicated in aggregation (Lee et al. 2005; Swaney et al. 2010). Among the other four genes, *splA* and *DDB_G0283893* are likely false positives. *splA* is dispensable for aggregation (Nuckolls et al. 1996), and the two mutant strains that carry *splA* mutations also harbor mutations in known aggregation-related genes that could account for the observed phenotypes. Moreover, as larger genes are more likely to be mutated at random, a statistical test indicates that the two mutations in *DDB_G0283893* were likely to occur by chance (binomial distribution, P value = 0.058). In summary, we identified 14 known aggregation-related genes in the screen for aggregation defects, supporting our expectation and suggesting that it is possible to identify recurrent mutations in a genetic screen over a large relevant target size. If we were studying an unknown pathway, we would need to achieve saturation to identify most of the genes, but even our limited screen has implicated two new genes as potential aggregation-related genes.

Multiple alleles reveal 13 suppressors of the *tgrB1–C1* mismatch phenotype

We recovered 63 mutants that suppressed the morphological and sporulation defects of the *tgrB1-C1* mismatch phenotype (Table 1). Many of the mutants were nearly indistinguishable from the wild type (Fig. 4A). The sequencing results revealed 79 genes that were mutated ≥2 times. Gene Ontology (GO) enrichment analysis of these genes suggests that six (*htt, lmpB, lysA, talA, tgrB1*, and *rapgapB*) are involved in cell-cell adhesion (P value = 0.0001, FDR = 0.0265). Thirteen genes were mutated ≥3 times (Fig. 3; Supplemental Table S1). Indeed, we identified 19 mutations in *rapgapB* and nine mutations in *tgrB1*, suggesting that our screen has been carried to near-saturation. These results suggest that our

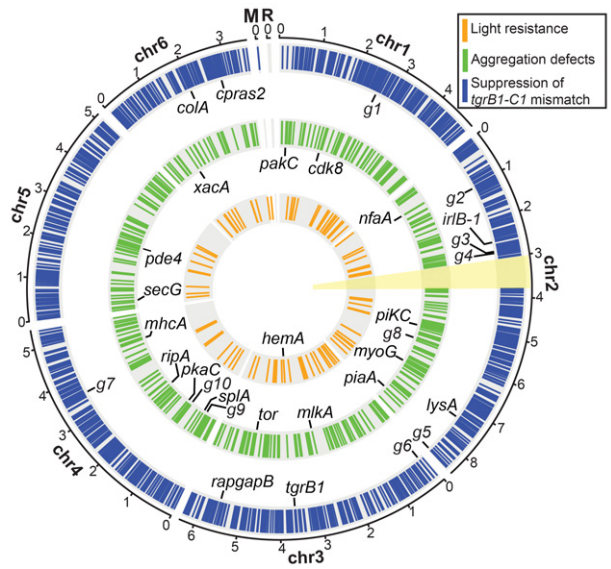

Figure 3. The genomic distribution of chemically induced mutations. The circular plot summarizes the distribution of chemically induced mutations in the six chromosomal (Chr 1–6), mitochondrial (M), and ribosomal (R) DNAs. Colored bars on the three concentric circles represent the mutations found in the three genetic screens as indicated in the legend: suppression of the *tgrB1-C1* mismatch (blue, $n = 63$ strains), aggregation defects (green, $n = 14$ strains), and light resistance (orange, $n = 6$ strains). The candidate genes in the individual screens are labeled *inside* the respective circles, and the black lines indicate their chromosomal positions. Abbreviations: *g1*, *DDB_G0270488*; *g2*, *DDB_G0271904*; *g3*, *DDB_G0273247*; *g4*, *DDB_G0273385*; *g5*, *DDB_G0277749*; *g6*, *DDB_G0277997*; *g7*, *DDB*_G0285705; *g8*, *DDB_G0275861*; *g9*, *DDB_G0283339*; *g10*, *DDB*_G0283893. The yellow sector (around 3 o'clock) indicates the second copy of the Chromosome 2 duplication (Chr 2: 3016083…3768654), which was masked during the alignment of sequencing reads. The full list of mutations is detailed in Supplemental Data 1–3 and the candidate genes in Supplemental Table S1. The scale *outside* the circles shows positions in million base pairs (Mb).

method is useful in implicating genes in a genetic screen over a moderate relevant target size.

So far, we have relied on multiple alleles and on published results to validate our screen results. The highest numbers of alleles were found in *rapgapB* and *tgrB1*, and we know that TgrB1 and TgrC1 interact to regulate development (Hirose et al. 2015) and that *rapgapB* encodes a RapA GTPase regulatory protein B that regulates cell-cell and cell-substrate adhesion (Parkinson et al. 2009). This knowledge and the availability of molecular tools allowed us to perform direct causality tests of these mutations.

Lack of correlation between mutations and fine morphological phenotypes

We hypothesized that the mutants' morphological phenotypes would be instructive in analyzing the underlying mutations. We therefore analyzed the morphologies of 25 *tgrB1-C1*-mismatch-suppressor strains at seven time points over 36 h of development. The genotypes and phenotypes did not seem to correlate when visualized by multidimensional scaling (Supplemental Fig. S2), and analysis by multiple linear regressions found no significant association either (mutations in *rapgapB*, P value = 0.3128; mutations in *tgrB1*, P value = 0.5462; mutations in any of the 13 suppressor genes, P value = 0.0920). We conclude that fine morphological phenotyping did not help to group mutants with similar suppressor mutations in this context.

Dominant causative mutations in *tgrB1*

Most of the mutations in *tgrB1* restored sporulation efficiency to near wild-type levels (Fig. 4A). Two mutant alleles, $tgrB1^{G275D}$ and $tgrB1^{G307D}$, independently arose twice and three times, respectively, in our screen (Supplemental Table S1). Both mutations (G275D and G307D) occurred in the invariable part of the first immunoglobulin-like domain in the extracellular region of the TgrB1 protein (Fig. 4B). We hypothesized that $tgrB1^{G275D}$ and $tgrB1^{G307D}$ are gain-of-function alleles because deletion of *tgrB1* confers only weak suppression of the sporulation defect in $tgrC1^{-}$ cells (Benabentos et al. 2009). We therefore tested whether expressing $tgrB1^{G275D}$ or $tgrB1^{G307D}$ driven by the native *tgrB1* promoter would suppress the phenotypic defects of three mutants: the parental mismatch strain $tgrB1^{AX4}tgrC1^{QS38}$, the single-gene deletion strain $tgrC1^{-}$, and the double-gene deletion strain $tgrB1^{-}tgrC1^{-}$ (Fig. 4C). We found that transformation with either of the two mutant *tgrB1* alleles strongly suppressed the sporulation defects, whereas the wild-type allele $tgrB1^{WT}$ did not (Fig. 4C). These results suggest that the G275D and G307D mutations in *tgrB1* were indeed the causative mutations in the original strains and that both alleles are dominant.

Recessive causative mutations in *rapgapB*

To characterize the *rapgapB* alleles, we tried to complement the original suppressor mutant strains by transformation with wild-type *rapgapB*. We transformed the $rapgapB^{WT}$ allele, driven by its native promoter, into mutants carrying the mutated *rapgapB* (Fig. 5A,B). We grew the transformants in association with bacteria on nutrient agar and counted plaques that lost the suppression phenotype (Fig. 5B). We found that the majority of plaques in NTG82 (70%, $rapgapB^{M1I}$) and NTG14 (90%, $rapgapB^{G382D}$) exhibited a loose-aggregate phenotype, which is the *tgrB1-C1* mismatch phenotype. This finding indicates that M1I and G382D are recessive causative mutations of the phenotypic suppression. In contrast, transformation with $rapgapB^{WT}$ did not affect the suppression phenotype of NTG09 (0%, $rapgapB^{G191D}$) and NTG64 (0%, $rapgapB^{Q44*}$) (Fig. 5B). A likely explanation is that these two variants are dominant causative alleles, but it is possible that other mutations in these genomes caused the phenotypic suppression.

Altogether, the genetic analyses of *tgrB1* and *rapgapB* support the hypothesis that multiple independent alleles implicate specific genes in this type of genetic screen. They also illustrate the power of the method to generate a broad spectrum of mutations.

Discussion

Our findings show that chemical mutagenesis followed by whole-genome sequencing can reveal a broad spectrum of causative mutations in genetic screens. The key technical feature is the low level of mutagenesis, with 10%–50% survival and 20–30 SNVs per genome. The key conceptual feature is the implication of a single common gene by multiple independent mutations. Mutations outside of the implicated gene help to distinguish independent mutants from siblings. We used complementation with expression vectors to validate our conclusions. This step is not necessary in future screens, but complementation is a useful tool for analyzing the genetic nature of the mutated alleles.

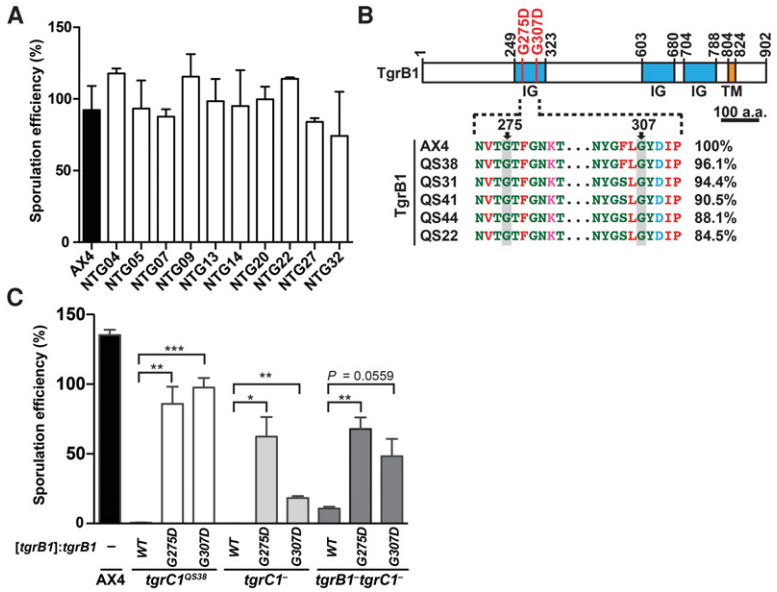

Figure 4. Dominant causative mutations in *tgrB1* identified in the screen for suppression of the *tgrB1-C1* mismatch phenotype. (*A*) We developed cells for 72 h on a nitrocellulose filter and counted the fraction (%) of cells that formed spores. Strain names are indicated *under* the *x*-axis: AX4 cells (black bar) and 10 NTG-mutagenized mutants (white bars) isolated from the screen for suppression of the *tgrB1-C1* mismatch phenotype. The bar graph represents the mean ± standard deviation (SD) of three independent replicates. (*B*) (*Top*) TgrB1 contains three immunoglobulin-like domains (IG, blue) and one transmembrane domain (TM, orange). Numbers *above* the chart represent amino acid positions. Scale bar = 100 aa. Recurrent missense mutations (G275D and G307D) are indicated as red bars. (*Bottom*) Partial protein sequence alignment of the polymorphic *tgrB1* alleles from AX4 and five wild isolates as indicated. The pairwise sequence identity (%) compared to $TgrB1^{AX4}$ is indicated on the *right*. (*C*) We expressed three different alleles ($tgrB1^{WT}$, $tgrB1^{G275D}$, or $tgrB1^{G307D}$, as indicated immediately *below* the *x*-axis) driven by the native promoter, in three *tgrC1*-defective mutants ($tgrC1^{QS38}$, $tgrC1^{-}$, and $tgrB1^{-}tgrC1^{-}$, as indicated on the *bottom*). We allowed the cells to develop and measured their sporulation efficiencies as the proportion of cells (%) that formed spores (*y*-axis). Bars represent the means ± SD of four independent replicates. Welch's unequal variances *t*-test (two-tailed): (*) *P* value < 0.05; (**) *P* value < 0.01; (***) *P* value < 0.005.

Previous chemical mutagenesis studies were done mostly at high levels of mutagenesis and at ~0.1% survival. These rates were interpreted as an indication that mutagenesis resulted in an average of seven lethal hits per genome (Loomis 1978, 1987). We have observed a diminishing returns relationship between the killing rate and the number of SNVs per genome, suggesting that lethality in previous studies was compounded by toxicity. Regardless, the conditions we used are suitable for large-scale screens. With 20 genic mutations per genome, the odds of mutating any one of the 12,000 genes in one *Dictyostelium* genome are 1:600. A typical mutagenesis reaction produces approximately 10^7 mutants, enough to saturate almost any gene. Remarkably, the number of SNVs per genome is rather homogeneous, which makes the downstream analysis rather convenient.

High-throughput sequencing was not available in the 1970s, and genetic mapping in *Dictyostelium* is difficult, so most mutations were never characterized in molecular detail. The presumed large number of mutations per genome also resulted in confounding effects, with a 50% chance that secondary mutations affected the studied phenotype (Loomis 1987). Therefore, researchers had to perform genetic crosses and to study several mutants in order to associate genotypes with phenotypes (Newell 1978). Here, we implicated genes by identifying multiple independent alleles in genome sequencing data without genetic mapping. Another observation in previous studies was that most mutations were recessive (Loomis 1987). Our findings indicate that chemical mutagenesis produces dominant alleles as well.

Some analyses of chemical mutagenesis data were based on the assumption that mutations occur at random (Loomis 1987). These analyses were remarkably accurate despite our finding that NTG mutagenesis is biased toward exons of coding genes. This bias is a combined result of the skewed nucleotide content of the *Dictyostelium* genome (Eichinger et al. 2005) and the preference of NTG to alkylate guanine residues (Ohta 2000). Nevertheless, NTG mutagenesis seems to be unbiased at the genome level, as all the genes appear to be equally susceptible. The bias to coding exons is convenient because mutations in these sequences are somewhat simpler to interpret. Compared to other mutagenesis methods, such as REMI (Kuspa and Loomis 1992), antisense RNA (Spann et al. 1996), and RNA interference (Kuhlmann et al. 2006), our method provides a broader spectrum of mutations and opens the field to exploration of modifications that are not necessarily null or loss-of-function mutations. For example, NTG mutagenesis can generate temperature sensitive alleles (Loomis 1969; Liwerant and Pereira Da Silva 1975), and we found strong suppressors of the *tgrB1-tgrC1* mismatch phenotype, which were not found by REMI screens (Li et al. 2015; Wang and Shaulsky 2015). Some mutations, such as the dominant alleles of *tgrB1*, cannot be produced by REMI. The mutation spectrum could be broadened further by using UV irradiation and other chemicals that have been tested in *Dictyostelium* (Liwerant and Pereira Da Silva 1975). According to the central repository of *Dictyostelium* genomic data (dictyBase, April 2016 [Fey et al. 2013]), ~11% of the *Dictyostelium* genes have been mutated by REMI or by methods such as homologous recombination. Most of these mutations conferred loss-of-function. Using the method described here is expected to increase the number of mutated genes and the variety of available mutations, opening the field of functional genomics in *Dictyostelium* to new exploration.

Important considerations in genetic screens are the relevant target size and saturation. Target size is a function of the number of genes that participate in a biological process and the size of each gene. We tested our method on three phenotypes: Resistance to light was presumed to have a small target size (approximately 1–5 genes), defective aggregation was known to have a large target size (approximately 100 genes), and suppression of the *tgrB1-tgrC1* mismatch had an unknown target size that turned out to be in the middle (approximately 10–20 genes). As expected, saturation was achieved in the small and middle size screens and not in the large size one. Our method relies on saturation because we can only implicate genes that are independently mutated several times. There is no theoretical way to predict the relevant target size, but chemical mutagenesis can be used to

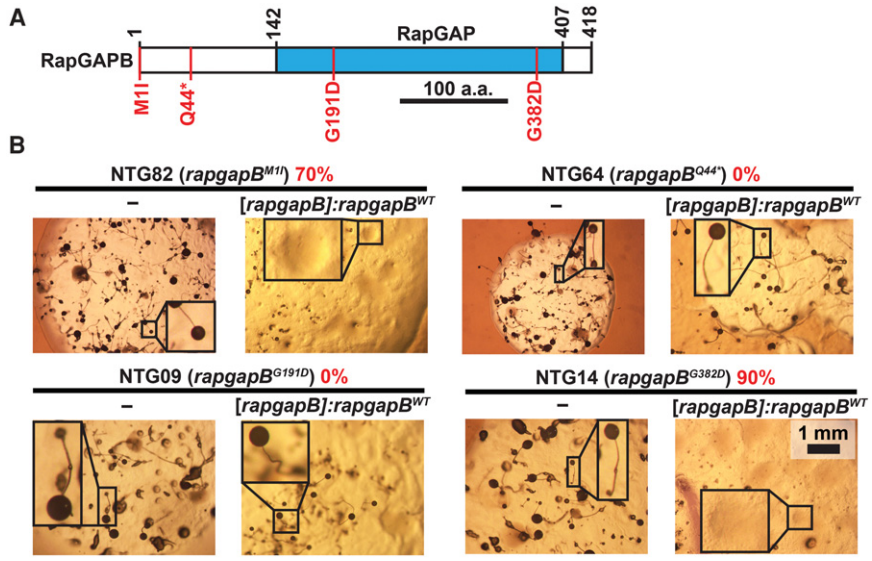

Figure 5. Recessive causative mutations in *rapgapB* observed in the screen for suppression of the *tgrB1-C1* mismatch phenotype. (*A*) Schematic representation of RapGAPB. The blue rectangle indicates the Rap GTPase-activating protein (RapGAP) domain. Numbers *above* the chart represent amino acid positions. Scale bar = 100 aa. Four of the 17 amino acid substitutions observed in the screen are indicated in red (M1I, Q44*, G191D, and G382D). (*B*) We performed a complementation test by introducing the *rapgapB*^{WT} allele driven by the endogenous promoter ([*rapgapB*]:*rapgapB*^{WT}) into chemically mutagenized strains carrying the indicated *rapgapB* mutations. We grew the transformants in association with bacteria on nutrient agar and measured the proportion of colonies that lost the suppression phenotype (%, red text). We photographed the morphology of the mutants with or without the *rapgapB*^{WT} expression construct, as indicated *below* the line of each panel. The names of the individual strains (NTG#) and the respective *rapgapB* mutations are indicated *above* the line in each panel. *Insets* are magnified (3×). Scale bar = 1 mm.

estimate the number of genes required in any biological process (Loomis 1987).

In terms of cost and efficiency, our method relies on economies of scale. Generating mutants is inexpensive and fast, whereas the screen or selection phase depends on the experimental design. In the sequencing phase, we used 16- to 24-fold multiplexing, generating an average of 20-fold sequence coverage. We discovered ~90% of the mutations in the coding regions in our screens (Supplemental Fig. S1B), and we estimate that doubling the multiplexing would allow discovery of ~80%. This compromise may be acceptable depending on the application. The commercial cost of sequencing in the United States on January 2016 was roughly $2500–$4000 per lane. This cost can be considerably lower through institutional core services, and it is likely to decline in the future. We note that next-generation sequencing data management and analysis can be expensive, too, but the cost can be reduced through use of shared institutional resources or public free cloud platforms, such as Galaxy (https://usegalaxy.org). Our method is therefore accessible to laboratories with modest budgets.

The large number of mutants generated by NTG mutagenesis and the advantage of working with a microbial system makes the method applicable to genetic screens as well as selections. Each approach has advantages and disadvantages (Shuman and Silhavy 2003), but our findings indicate that either approach, or a combination thereof, can be used. Genetic suppression is a powerful tool in *Dictyostelium* (Shaulsky et al. 1996), and our method is suitable for this type of investigation as well. More importantly, the ease of NTG mutagenesis makes it applicable to nonaxenic strains (Loomis 1987), where transformation-based methods are possible but somewhat difficult (Veltman et al. 2014). Our method could also be readily adapted to any haploid organism with a small, sequenced genome, including many amoebae, fungi, and bacteria.

Methods

Genetic screens by chemical mutagenesis

We performed chemical mutagenesis as described (Loomis 1987) with minor modifications. The stock solution of *N*-methyl-*N*′-nitro-*N*-nitrosoguanidine (NTG, Pfaltz&Bauer) was prepared in DMSO at 10 mg/mL and stored as 100 µL aliquots for one-time use at −80°C. We harvested exponentially growing *Dictyostelium* cells and washed once with KK2 buffer (16.3 mM KH_2PO_4 and 3.7 mM K_2HPO_4). We mutagenized 10^8 cells in 1 mL of KK2 buffer containing 500 µg/mL of NTG for 10, 20, 30, 40, or 60 min. Afterward, we collected the cells by centrifugation at 500*g* for 30 sec and resuspended in 10 mL HL5 medium. We estimated the survival rate by plating 100 to 10,000 cells on SM plates in association with *Klebsiella aerogenes*. We plated the rest of the mutagenized cells on SM plates with bacteria at a density of 10^3 to 10^7 cells per 10-cm plate. For aggregation defects, we inspected plaques under a stereomicroscope for strains that did not form streams and mounds. For light resistance, we selected for mutagenized AX4 cells that grew and developed under constant exposure to 5000 to 10,000 lux of light (Mastech light meter) illuminated with compact fluorescent light (CFL) bulbs (GE 100-Watt daylight 6500K). Ten separate pools of 10^6 mutagenized cells were selected in this case, and we isolated only one stable mutant from each population to avoid siblings. For the suppression of the *tgrB1-C1* mismatch, we grew mutagenized *tgrB1*^{AX4}*tgrC1*^{QS38} cells on SM plates with bacteria and allowed them to develop for 3 d after clearing the plate. We collected the cells and treated them with detergent (0.1% NP-40 and 10 mM EDTA) to kill nonspore cells. We plated the surviving spores on fresh SM plates with bacteria, followed by screening for fruiting body-forming plaques.

Genomic DNA sequencing

We prepared genomic DNA (gDNA) as described (Santhanam et al. 2015). Briefly, we harvested 10^8–10^9 cells grown in HL5 medium, followed by washing once with KK2 buffer. We lysed the cells in 10 mL of nuclei buffer (40 mM Tris-HCl pH 7.8, 1.5% sucrose, 0.1 mM EDTA, 6 mM $MgCl_2$, 40 mM KCl, 5 mM DTT, and 0.4% NP40) on ice for 10 min. We collected the nuclei by centrifuging at 20,000*g* for 10 min. We incubated the nuclei in 500 µL of STE/SDS/Protease K solution (450 µL STE solution [10 mM Tris-HCl pH 8.0, 10 mM EDTA, and 400 mM NaCl], 25 µL 20% SDS, 15 µL ddH_2O, and 10 µL of 10 mg/mL Proteinase K) at 60°C for 1 h. We performed phenol/chloroform extraction and ethanol precipitation and repeated the process once more after treating the gDNA with RNase A. For library preparation, we sheared 1 µg of gDNA in 100 µL of ddH_2O in a Covaris microTUBE (#520052) by Covaris S220 Focused-ultrasonicator (60 sec, 10% duty cycle, 200 cycles per burst, 14W acoustic power, 7°C). The rest of the library

preparation was performed as described for cDNA library preparation (Miranda et al. 2013). We quantified individual gDNA libraries by quantitative PCR to determine the PCR cycle number for enriching and barcoding with indexing primers (Meyer and Kircher 2010; Miranda et al. 2013). We multiplexed 16–24 barcoded samples on one lane for 100-bp paired-end sequencing on the Illumina HiSeq 2000 platform.

Sequence read alignment and variant detection

We demultiplexed the sequencing reads based on the barcodes and mapped the processed reads to the reference *Dictyostelium* AX4 genome by the BWA-MEM (Li and Durbin 2009) algorithm (version 0.7.5a) using default parameters. For all of the analyses, we masked one copy of the 750-kb duplication on Chromosome 2 (position 3016083 to 3768654) in the reference genome (Eichinger et al. 2005). For strains carrying the foreign $tgrC1^{QS38}$ allele, we replaced the $tgrC1^{AX4}$ allele with the $tgrC1^{QS38}$ allele in the reference genome. After read alignment, we used Picard tools (version 1.119) to mark and remove duplicates (paired-end reads that carried identical sequence information and most likely arose at the indexing PCR step of the library preparation). We evaluated the quality statistics of the mapped reads with Qualimap (version 2.1.1) (García-Alcalde et al. 2012). Subsequently, we detected single nucleotide variants and indels by performing multisample variant calling with the Genome Analysis Toolkit's Unified Genotyper (GATK version 3.4–46) (McKenna et al. 2010). In variant calling, we considered the duplication on Chromosome 2 as a diploid genome and the rest of the chromosomal regions as a haploid genome. All of the raw reads, aligned reads, and VCF files can be accessed on dictyExpress (https://dictyexpress.research.bcm.edu/genboard/#/chemical-mutagenesis/). We created the circular plot in Figure 3 with the R package OmicCircos (Hu et al. 2014).

Filtering variants

We applied several filters to the raw SNVs and indels called by GATK. First, a locus must be covered by at least five sequencing reads. Secondly, a locus in the haploid *Dictyostelium* genome can only carry one allele at a time. We considered an allele at a given locus to be the one supported by ≥80% of the reads. If there was no allele that passed the threshold, we discarded the locus. Third, a locus on the Chromosome 2 duplication can carry two alleles. We considered the locus to be heterozygous if the two alleles were both supported by 40% to 60% of the reads. Lastly, we filtered the variants detected in the chemically mutagenized strains against the pre-existing variants in the relevant parental strain. The full list of filtered variants in this study is summarized in Supplemental Data 1–3. R codes for variant filtering can be found on the GitHub repository (https://github.com/chenglinli/chemical_mutagenesis) and in Supplemental File 1.

Genetic constructs

To construct the $rapgapB^{WT}$ expression vector, we PCR-amplified a 3-kb DNA fragment including the *rapgapB* gene (1.6 kb), 5′ promoter region (0.8 kb), and 3′ region (0.6 kb) with the following primers: 5′-ATTATCTTTGTGGGTTTAGTTGTG-3′ and 5′-TGATGCTG AACCTCTTGATATG-3′. We cloned the 3-kb fragment into the pCR-Blunt II-TOPO vector (ThermoFisher Scientific), followed by subcloning into the EcoRV and BamHI sites of the pLPBLP vector (Faix et al. 2004). The $tgrB1^{WT}$ expression construct, in which expression was driven by the native promoter, was kindly provided by S. Hirose. We replaced the wild-type allele $tgrB1^{AX4}$ with the mutated alleles $tgrB1^{G275D}$ and $tgrB1^{G307D}$ by cutting and pasting PCR-amplified mutant *tgrB1* alleles with EcoNI and AgeI. The primers for amplifying the mutant *tgrB1* alleles were 5′-AAA TGGATACAAATGGAG-3′ and 5′-TTACAGTCATATTCTTAACA CC-3′.

Phenotyping

To group the *Dictyostelium* strains based on their developmental morphology, we developed individual strains on a 1.5% nonnutrient KK2 agar containing 500 µL/mL streptomycin. We took pictures of the developmental morphology from above under a stereomicroscope at seven time points (8, 10, 12, 16, 20, 24, and 36 h). We scored the morphology at each time point based on the predominant developmental structures. The scores for individual structures were 1 for ripples, 2 for streaming, 3 for loose aggregates, 4 for tight aggregates, 5 for tipped mounds, 6 for slugs and fingers, 7 for Mexican hats, 8 for early culmination, 9 for mid-culmination, and 10 for fruiting bodies. We calculated the pairwise distances between the strains by aligning the time series with the dynamic time warping (DTW) algorithm (Sakoe and Chiba 1978), while computing the distance between the two morphological states as the absolute difference between the scores for their corresponding predominant structures. The time-shift penalty for DTW was set to 0.2. In addition to morphology, we quantified the sorus size of individual strains after growth and development on SM plates in association with *Klebsiella aerogenes*, but this information was not included in the distance calculation. To measure sporulation efficiency, we developed a known number of cells for 48 h, collected spores, and counted them with phase contrast microscopy. Sporulation efficiency was calculated as the fraction (%) of cells that became spores.

Data access

The whole-genome sequence data from this study have been submitted to the NCBI Sequence Read Archive (SRA; http://www.ncbi.nlm.nih.gov/sra/) under accession number SRP073746.

Acknowledgments

We thank R. Sucgang and A. Kuspa for helpful suggestions and insightful discussions, A. Kuspa and R. Gomer for critical review of the manuscript, S. Hirose for the $tgrB1^{WT}$ expression construct, and M. Katoh-Kurasawa for technical guidance with whole-genome sequencing. This work was supported by National Institutes of Health (NIH) grants R01 GM084992 and P01 HD03691, and A.N.W. was partly supported by grant T32 GM008307 from the NIH; C.F.L. was partly supported by the Burroughs Wellcome Fund through the Houston Laboratory and Population Sciences Training Program in Gene-Environment.

Author contributions: C.F.L. and G.S. conceived and designed the experiments. C.F.L. performed the experiments and analyzed the data. B.S. participated in the development of the genome analysis code, A.N.W. photographed the developmental structures, and B.Z. developed and implemented the dynamic time warping algorithm for morphological phenotyping. C.F.L. and G.S. wrote the manuscript.

References

Ajioka RS, Phillips JD, Kushner JP. 2006. Biosynthesis of heme in mammals. *Biochim Biophys Acta* **1763:** 723–736.

Annesley SJ, Fisher PR. 2009. *Dictyostelium discoideum*—a model for many reasons. *Mol Cell Biochem* **329:** 73–91.

Benabentos R, Hirose S, Sucgang R, Curk T, Katoh M, Ostrowski EA, Strassmann JE, Queller DC, Zupan B, Shaulsky G, et al. 2009.

Polymorphic members of the *lag* gene family mediate kin discrimination in *Dictyostelium*. *Curr Biol* **19:** 567–572.
Chen G, Wang J, Xu X, Wu X, Piao R, Siu C-H. 2013. TgrC1 mediates cell–cell adhesion by interacting with TgrB1 via mutual IPT/TIG domains during development of *Dictyostelium discoideum*. *Biochem J* **452:** 259–269.
Dolmans DEJGJ, Fukumura D, Jain RK. 2003. Timeline: Photodynamic therapy for cancer. *Nat Rev Cancer* **3:** 380–387.
Eichinger L, Pachebat JA, Glöckner G, Rajandream M, Sucgang R, Berriman M, Song J, Olsen R, Szafranski K, Xu Q, et al. 2005. The genome of the social amoeba *Dictyostelium discoideum*. *Nature* **435:** 43–57.
Faix J, Kreppel L, Shaulsky G, Schleicher M, Kimmel AR. 2004. A rapid and efficient method to generate multiple gene disruptions in *Dictyostelium discoideum* using a single selectable marker and the Cre-*loxP* system. *Nucleic Acids Res* **32:** e143.
Fey P, Dodson RJ, Basu S, Chisholm RL. 2013. One stop shop for everything *Dictyostelium*: dictyBase and the Dicty Stock Center in 2012. *Methods Mol Biol* **983:** 59–92.
García-Alcalde F, Okonechnikov K, Carbonell J, Cruz LM, Götz S, Tarazona S, Dopazo J, Meyer TF, Conesa A. 2012. Qualimap: evaluating next-generation sequencing alignment data. *Bioinformatics* **28:** 2678–2679.
Godley BF, Shamsi FA, Liang F-Q, Jarrett SG, Davies S, Boulton M. 2005. Blue light induces mitochondrial DNA damage and free radical production in epithelial cells. *J Biol Chem* **280:** 21061–21066.
Haelterman NA, Jiang L, Li Y, Bayat V, Sandoval H, Ugur B, Tan KL, Zhang K, Bei D, Xiong B, et al. 2014. Large-scale identification of chemically induced mutations in *Drosophila melanogaster*. *Genome Res* **24:** 1707–1718.
Hirose S, Benabentos R, Ho H-I, Kuspa A, Shaulsky G. 2011. Self-recognition in social amoebae is mediated by allelic pairs of tiger genes. *Science* **333:** 467–470.
Hirose S, Santhanam B, Katoh-Kurosawa M, Shaulsky G, Kuspa A. 2015. Allorecognition, via TgrB1 and TgrC1, mediates the transition from unicellularity to multicellularity in the social amoeba *Dictyostelium discoideum*. *Development* **142:** 3561–3570.
Hu Y, Yan C, Hsu C, Chen Q, Niu K, Komatsoulis GA, Meerzaman D. 2014. OmicCircos: a simple-to-use R package for the circular visualization of multidimensional omics data. *Cancer Inform* **13:** 13–20.
Kuhlmann M, Popova B, Nellen W. 2006. RNA interference and antisense-mediated gene silencing in *Dictyostelium*. In *Dictyostelium discoideum protocols* (ed. Eichinger L, Rivero F), Vol. 346, pp. 211–226. Humana Press, New Jersey.
Kuspa A, Loomis WF. 1992. Tagging developmental genes in *Dictyostelium* by restriction enzyme-mediated integration of plasmid DNA. *Proc Natl Acad Sci* **89:** 8803–8807.
Lee S, Comer FI, Sasaki A, McLeod IX, Duong Y, Okumura K, Yates JR, Parent CA, Firtel RA. 2005. TOR complex 2 integrates cell movement during chemotaxis and signal relay in *Dictyostelium*. *Mol Biol Cell* **16:** 4572–4583.
Li H, Durbin R. 2009. Fast and accurate short read alignment with Burrows–Wheeler transform. *Bioinformatics* **25:** 1754–1760.
Li C-LF, Chen G, Webb AN, Shaulsky G. 2015. Altered *N*-glycosylation modulates TgrB1- and TgrC1-mediated development but not allorecognition in *Dictyostelium*. *J Cell Sci* **128:** 3990–3996.
Liwerant IJ, Pereira Da Silva LH. 1975. Comparative mutagenic effects of ethyl methanesulfonate, *N*-methyl-*N*′-nitro-*N*-nitrosoguanidine, ultraviolet radiation and caffeine on *Dictyostelium discoideum*. *Mutat Res* **33:** 135–146.
Loomis WF. 1969. Temperature-sensitive mutants of *Dictyostelium discoideum*. *J Bacteriol* **99:** 65–69.
Loomis WF. 1978. The number of developmental genes in *Dictyostelium*. *Birth Defects Orig Artic Ser* **14:** 497–505.
Loomis WF. 1987. Chapter 3 - Genetic tools for *Dictyostelium discoideum*. In *Methods in cell biology* (ed. Spudich JA), Vol. 28, pp. 31–65. Academic Press, New York.
Lucchesi P, Carraway M, Marinus MG. 1986. Analysis of forward mutations induced by *N*-methyl-*N*′-nitro-*N*-nitrosoguanidine in the bacteriophage P22 *mnt* repressor gene. *J Bacteriol* **166:** 34–37.
McKenna A, Hanna M, Banks E, Sivachenko A, Cibulskis K, Kernytsky A, Garimella K, Altshuler D, Gabriel S, Daly M, et al. 2010. The Genome Analysis Toolkit: a MapReduce framework for analyzing next-generation DNA sequencing data. *Genome Res* **20:** 1297–1303.
Meyer M, Kircher M. 2010. Illumina sequencing library preparation for highly multiplexed target capture and sequencing. *Cold Spring Harb Protoc* **2010:** ppdb.prot5448.
Miranda ER, Rot G, Toplak M, Santhanam B, Curk T, Shaulsky G, Zupan B. 2013. Transcriptional profiling of *Dictyostelium* with RNA sequencing. *Methods Mol Biol* **983:** 139–171.
Newell PC. 1978. Genetics of the cellular slime molds. *Annu Rev Genet* **12:** 69–93.
Nuckolls GH, Osherov N, Loomis WF, Spudich JA. 1996. The *Dictyostelium* dual-specificity kinase splA is essential for spore differentiation. *Development* **122:** 3295–3305.
Ohta T. 2000. A comparison of mutation spectra detected by the *Escherichia coli* Lac^+ reversion assay and the *Salmonella typhimurium* His^+ reversion assay. *Mutagenesis* **15:** 317–323.
Parkinson K, Bolourani P, Traynor D, Aldren NL, Kay RR, Weeks G, Thompson CRL. 2009. Regulation of Rap1 activity is required for differential adhesion, cell-type patterning and morphogenesis in *Dictyostelium*. *J Cell Sci* **122:** 335–344.
Sakoe H, Chiba S. 1978. Dynamic programming algorithm optimization for spoken word recognition. *IEEE Trans Acoust ASSP* **26:** 43–49.
Santhanam B, Cai H, Devreotes PN, Shaulsky G, Katoh-Kurasawa M. 2015. The GATA transcription factor GtaC regulates early developmental gene expression dynamics in *Dictyostelium*. *Nat Commun* **6:** 7551.
Sarin S, Prabhu S, O'Meara MM, Pe'er I, Hobert O. 2008. *Caenorhabditis elegans* mutant allele identification by whole-genome sequencing. *Nat Methods* **5:** 865–867.
Shaulsky G, Escalante R, Loomis WF. 1996. Developmental signal transduction pathways uncovered by genetic suppressors. *Proc Natl Acad Sci* **93:** 15260–15265.
Shuman HA, Silhavy TJ. 2003. Microbial genetics: The art and design of genetic screens: *Escherichia coli*. *Nat Rev Genet* **4:** 419–431.
Spann TP, Brock DA, Lindsey DF, Wood SA, Gomer RH. 1996. Mutagenesis and gene identification in *Dictyostelium* by shotgun antisense. *Proc Natl Acad Sci* **93:** 5003–5007.
Swaney KF, Huang C-H, Devreotes PN. 2010. Eukaryotic chemotaxis: a network of signaling pathways controls motility, directional sensing, and polarity. *Annu Rev Biophys* **39:** 265–289.
Veltman DM, Lemieux MG, Knecht DA, Insall RH. 2014. PIP_3-dependent macropinocytosis is incompatible with chemotaxis. *J Cell Biol* **204:** 497–505.
Wang Y, Shaulsky G. 2015. TgrC1 has distinct functions in *Dictyostelium* development and allorecognition. *PLoS One* **10:** e0124270.
Williams JG. 2010. *Dictyostelium* finds new roles to model. *Genetics* **185:** 717–726.
Williams KL, Newell PC. 1976. A genetic study of aggregation in the cellular slime mould *Dictyostelium discoideum* using complementation analysis. *Genetics* **82:** 287–307.

Received February 17, 2016; accepted in revised form May 17, 2016.